Characterization of Damp-Heat Degradation of $CuInGaSe_2$ Solar Cell Components and Devices by (Electrochemical) Impedance Spectroscopy

Preprint

F.J. John Pern and Rommel Noufi

Presented at SPIE Optics + Photonics 2011
San Diego, California
August 21-25, 2011

Conference Paper
NREL/CP-5200-52564
September 2011

Contract No. DE-AC36-08GO28308

NOTICE

Available electronically at http://www.osti.gov/bridge

Available for a processing fee to U.S. Department of Energy
and its contractors, in paper, from:

U.S. Department of Energy
Office of Scientific and Technical Information

P.O. Box 62
Oak Ridge, TN 37831-0062
phone: 865.576.8401
fax: 865.576.5728
email: mailto:reports@adonis.osti.gov

Available for sale to the public, in paper, from:

U.S. Department of Commerce
National Technical Information Service
5285 Port Royal Road
Springfield, VA 22161
phone: 800.553.6847
fax: 703.605.6900
email: orders@ntis.fedworld.gov
online ordering: http://www.ntis.gov/help/ordermethods.aspx

Cover Photos: (left to right) PIX 16416, PIX 17423, PIX 16560, PIX 17613, PIX 17436, PIX 17721

Printed on paper containing at least 50% wastepaper, including 10% post consumer waste.

CHARACTERIZATION of damp-heat degradation of $CuInGaSe_2$ solar cell components and devices by (electrochemical) impedance spectroscopy

F.J. John Pern and Rommel Noufi
National Center for Photovoltaics, National Renewable Energy Laboratory
1617 Cole Blvd., Golden, CO, USA 80401

ABSTRACT

This work evaluated the capability of (electrochemical) impedance spectroscopy (IS, or ECIS as used here) to monitor damp heat (DH) stability of contact materials, $CuInGaSe_2$ (CIGS) solar cell components, and devices. Cell characteristics and its variation of the CIGS devices were also examined by the ECIS. Bare and encapsulated sample sets were separately prepared and exposed in an environmental chamber at 85°C and 85% relative humidity (RH). The ECIS results from bare samples tested within 50-100 h of DH exposure allowed the determination of the use of a conducting Ag paste and a low-melting-point solder alloy for making a DH-stable external connection with Au wires. Bare Mo and AlNi grid degraded (corroded) rapidly while Ni was DH-stable. The moisture-dampened Al-doped ZnO (AZO) and bilayer ZnO (BZO) likely underwent hydrolytic "capacitor-forming" reaction by DH, resulting in "transient" behavior of very high resistance in ECIS that was not detected by four-point probe. Using an encapsulation test structure that allowed moisture ingress control, DH-induced degradation (resistance increase) rates of BZO on glass decreased from 0.21 ohm/h using a moisture-permeable Tedlar/Polyester/Tedlar (TPT) backsheet to 1.0 x 10^{-3} ohm/h using a moisture barrier FG-200 film, while Mo on glass did not exhibit the same conducting degradation and corrosion as the bare samples after over 1270 h DH exposure. CIGS solar cells encapsulated with a TPT backsheet degraded irregularly over 774 h DH exposure. Key resistance and capacitance parameters extracted by curve fitting of impedance data clearly showed the variation and impact of DH exposure on cell characteristics. Profound "depression" or shorting of the "p-n junction capacitor" by DH was evident. ECIS results are shown to correlate reasonably well with the solar cells' current-voltage (I-V) degrading trends. Furthermore, ECIS analysis was capable of differentiating cell degradation due to "junction capacitor" shorting, damage or breakdown from that due to electrical conduction failure on AlNi/BZO layers.

Keywords: (electrochemical) impedance spectroscopy (ECIS), damp heat degradation, $CuInGaSe_2$ (CIGS) solar cell, AlNi contact grid, Al-doped ZnO, Mo base electrode, conducting silver paste.

1. INTRODUCTION

Long-term performance reliability is critical for all kinds of photovoltaic (PV) modules, including thin-film CIGS. For terrestrial thin-film modules, the IEC 61646 qualification standard requires a stringent DH test at 85°C and 85% relative humidity (RH) for 1000 h. A high percentage of thin-film modules reportedly failed in this test [1]. The CIGS cell component materials, including Mo, CIGS, and ZnO, have been shown to be DH-sensitive or unstable [2–8]. The CIGS solar cells or modules have also been shown to degrade in DH exposures [9-11]. A number of analytical and characterization methods are conventionally employed to measure and determine the solar cell performance and component materials degradation. For example, current-voltage (I-V) and quantum efficiency (QE) measurements are used to characterize solar cells, permitting a direct assess of the performance and spectral response of the solar cell. Photoluminescence (PL) and electroluminescence (EL) can be used to examine the recombination activity of minority carriers, allowing also a direct evaluation of the quality of the solar cells or mini-modules [12]. These methods are in general complementary. However, despite the ability to determine the key electrical parameters (i.e., open circuit voltage Voc, short circuit current density Jsc, fill factor FF, efficiency, dark current density J_o, and diode ideality factor n, along with the series resistance (Rs) and shunt resistance (Rsh)), the light/dark I-V measurement and curve analysis may not be able to provide clear insight or quantitative evaluation of how/why a solar cell has degraded by, for example, DH exposure.

In comparison, (electrochemical) impedance spectroscopy (IS or ECIS as preferably used here) is well known to be highly suitable for analyzing a variety of R-C circuits corresponding to a large number of chemical, electrochemical, and physical materials, devices, and/or systems [13]. Specifically, ECIS measurements can readily allow a quantitative evaluation of the electrical property of a solar cell's p-n junction, which is typically represented by an equivalent circuit of a parallel resistor and capacitor (i.e., "R-C" circuit model), and its series (contact/bulk) resistance. ECIS was employed to characterize the resistance and capacitance factors related to the minority carrier transport and performance of crystalline Si (c-Si) cells by Suresh [14] and Mora-Sero et al. [15]. A theoretical ECIS account of thin layer devices and extensive studies on the charge transfer dynamics of dye-sensitized solar cells have been given by J. Bisquert and his coworkers [15-17]. Along with the use of admittance spectroscopy, ECIS was used to characterize CIGS solar cells as reported by Bayhan and Kavasoglu [18,19]. Recently, we reported briefly its application to characterize CIGS solar cells and mini-modules as well as performance reliability of CIGS solar cells upon DH treatment [6,12]. Prior to this, its first use to characterize the DH stability of PV devices was reported for c-Si solar cells by Meier et al. at NREL [20]. Descriptions of the IS or ECIS technology are broadly available in literature, therefore no detailed elaboration is given here. Briefly, in a simplest form of the (EC)IS measurements, a small amplitude sinusoidal AC signal is applied to the subject of study with or without bias sweeping over a range of frequency, and the monitored real (Z') and imaginary (Z") impedance responses are displayed in a complex plane (Z" vs. Z') plot. A pure resistor will produce a vertical line, while an R-C circuit generates a semicircle. From the intercepts of the semicircle on the Z'(real) axis, series/bulk and charge transfer resistances can be determined. Capacitance can be then extracted from curve fitting. Corresponding Bode plots can be obtained as well. The majority of various solid-state solar cells including CIGS, where no mass transfer or diffusion of chemical or ionic species is involved so that slow-diffusion Warburg impedance is unimportant, can be modeled by a simple equivalent circuit as Scheme 1, comprising a series resistance (R_s') for contacts and bulk, a parallel resistance (R_p) for minority carrier recombination/diffusion and a capacitance (C) for diffusion and depletion [14-19]. (The symbol Rs' is used here to differ from the series resistance Rs obtained from solar cell's I-V measurement.) The circuit in Scheme 1 can also be called "Randles cell," one of the simplest cell models, and the complex plane plot can be called Nyquist plot, as commonly in electrochemistry. These parameters can be extracted by using curve fitting with an appropriate equivalent circuit for a solar cell system. The effective minority carrier lifetime or time constant can be calculated simply by the product of Rp*C or from the $\omega = 1/2\pi f$, where f is the maximum frequency derived from the semicircle of complex plane plot [16,17]. Degradation of the solar cells by environmental stresses can be therefore determined from changes in Rs', Rp, C, and Rp*C.

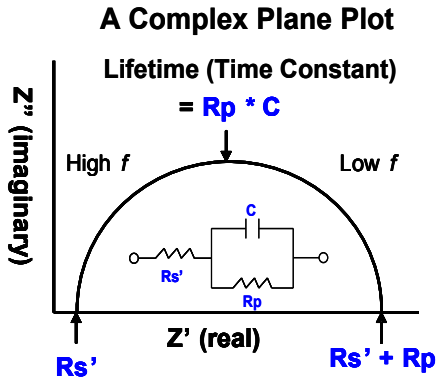

Scheme 1. Schematic representation of a simple equivalent circuit (insert), Rs'-(Rp-C), and its semicircle in the complex plane for a typical solar cell.

In this work, with the potential for *in-situ* monitoring, ECIS is being evaluated as a sensitive, non-invasive, non-destructive analytical method for monitoring the DH stability of the contact materials, CIGS solar cell components and devices. A quick screening was conducted for bare samples to determine the best materials and contact processing conditions prior to making DH-stable external contacts for samples to be encapsulated in a glass/Al fame test structure and subjected to longer-term stability study [6]. The obtained ECIS data are analyzed with curve fitting to extract key electrical IS parameters of degraded solar cells and correlate with I-V results as a function of DH exposure time, as well as to seek the possibility to differentiate or separate the degradation of the CIGS solar cells due to p-n junction shorting/breakdown from the degradation due to contact failure of bilayer ZnO and AlNi grid by DH.

2. EXPERIMENTAL

Sample preparations. Details for preparing the CIGS solar cells (cell area: 0.41 cm^2), single layer Al-doped ZnO (AZO) or bilayer ZnO (BZO, i.e., AZO on an intrinsic ZnO layer), the contact materials and contact processing for making external electrical connections to the tiny AlNi pad on CIGS solar cells, and the glass/edge sealant/Al frame/backsheet test structure for encapsulation were described in [6]. In this work, two more encapsulated samples, Dummy-1 and -2, with AZO, BZO and Mo on glass substrates, but no CIGS cell coupon, and a RH indicator strip were prepared in

addition to continue DH exposure for the "Set-5" with four CIGS cell coupons as reported in [6]. Dummy-1 used a Madico TPT backsheet for moisture ingress control, and "Dummy-2" used a moisture barrier film Barix FG-200, kindly provided by Techni-Met, Inc. All three were laminated at 100°C with TruSeal's SET LP01 gray edge sealant tape. The water vapor transmission rate (WVTR) is 142.77 g/m^2/day for the TPT backsheet, measured at 86.8°C with a breakthrough/equilibrium time at ~3 min/~15 min, and is < 10^{-3} g/m^2/day for the FG-200 barrier film (from product specifications).

For quick-screening the DH stability of contact materials and contacts, a matrix of bare (unencapsulated) samples having different contact designs was prepared: AZO and BZO on glass substrates with standard AlNi (0.05 μm Ni + 3 μm Al) or Ni-only (0.1–0.2 μm) grid patterns using a special interdigitated "bi-grid" for electrical (ECIS) measurements. These grided-AZO and BZO samples, and samples of AlNi, Ni-only, Mo film, and plain Ag paste coating on glass substrates, were first applied with a small dot of a Ag epoxy, Tra-Duct 2902 (TD2902) from Tra-Con, or a Ag paste, PV412 Solamet from DuPont, heated to dry, and attached with 4.5-mil Au wires with a low-melting-point solder alloy (Cerroseal35, or Cerro35 for short, In52/Sn48, from Cerro Corp.). Some BZO and Mo samples had the solder alloy directly applied on the sides and Au wires attached.

DH exposure. The exposure for the bare samples and the three encapsulated samples was conducted first in an ESPEC environment chamber at 85°C and 85% RH. In later stage, the three encapsulated samples were transferred to an AES environment chamber operating at the same DH conditions. A quick-screen test for the bare samples was exposed for 100 h. The encapsulated Set-5 and Dummy-1 and -2 were continued to 774 h and >1200 h, respectively. (The Set-5 was exposed for over 168 h when reported in [6].)

Characterization. As described previously in [6], I-V measurements were performed on an Optical Radiation Corp. model 1000 solar simulator, with QE on a custom-built system. ECIS measurements used an SI 1260 impedance/gain-phase analyzer and an SI 1286 electrochemical interface from Schlumberger Technologies, operated with the ZPlot and ZView software from Scribner Associates. A 10-mV amplitude AC voltage without a bias was used for all non-cell samples, and the scan frequency range started from 1M Hz to 1 Hz. For CIGS solar cells, the ECIS measurements were conducted in the dark. For the cells that showed a "jump" at 0.0V bias in the low-frequency range in the amplitude vs. frequency Bode plot, a 0.25V–0.30V forward bias was applied to obtain good Z" vs. Z' semicircles (see Section 3.3.1 below for details). The two built-in "instant fit" functions, Rs'-(Rp-C) and Rs'-(Rp-CPE), in the ZView were used directly for curve-fitting manually and individually the numerous data files (several hundreds) measured for the CIGS solar cells in Set-5. CPE stands for "constant phase element," a factor indicating the non-ideal quality of a capacitor [13,21,22]. The reported resistance and capacitance data are used directly without subtracting off the values contributed from the cables, alligators and Kevin probes, which are very low (≤ 0.01 ohm). Bare samples were also measured with a four-point probe for sheet resistance and examined with optical micro-imaging as needed.

3. RESULTS AND DISCUSSION

3.1 DH Stability of External Electrical Contact

Two issues are involved in this part: the needs for DH-stable contact materials and a simple processing method for making reliable, low-resistance external electrical contacts to the AlNi grid pad on the CIGS solar cells, which upon encapsulation cannot be accessed for repair if anything happens to the contact spots. Although the 3-μm Al offers high electrical conductivity, it is well known that Al surface is very difficult to apply solder alloy with dependable adhesion. Furthermore, the processing temperature has to be relatively low (preferably under 150°C) and the processing time relatively short (preferably under 20 min) in order to avoid causing thermal damage to the CIGS solar cells. Therefore, a conducting silver paste (PV412) and a two-part silver epoxy liquid (TD2902) were chosen and tested for their ability to deposit onto the surfaces of Al pad and other substrates at very small volume as a dot. The Ag paste PV412 was found more favorable for being easier to handle as well as its size control (without smearing or spread-out), and heat treatment (130°C for 8–10 min or 150°C for 5–8 min). Additionally, the dried Ag paste allows a solder alloy to be applied on with reasonable adhesion strength. A solder alloy, Cerro35, with a melting point of 118°C was found to meet the need when spot-applied onto the PV412 dot at 177°–200°C, the solder alloy dot then allowed the attachment of Au wire (4.5 mil diameter) by soldering with the same alloy. Another alloy with a melting point of 143°C (WS143, In97/Ag3, Williams Advanced Materials) was also determined suitable and later used. The various contacts are essentially resistors in nature;

each has a resistance and produces a relatively vertical, linear curve in the ECIS measurements (capacitance is assumed to be negligible). The resistance can simply use the Z'(real) impedance value at 1 Hz. Figure 1a gives the quick-screen results for the PV412, TD2902, and Cerro35 attached with Au wires on different substrates and exposed to DH for 100 h, showing low resistance and good DH stability of PV412/Cerro35/Au wire combination. Figure 1b shows the good DH stability of PV412 Ag paste coated on glass microslides as measured with a four-point probe, confirming DuPont's materials data sheet of high DH stability for PV412. The results hence established the simple processing conditions with materials that are DH-stable for making contact to the AlNi pad. The contact structure represented by layer would be: Ni/Al/PV412/Cerror35/Au wire, first heated at 150°C for ~6 min for PV412 and then soldered at 177-190°C for Cerro35 (or WS143).

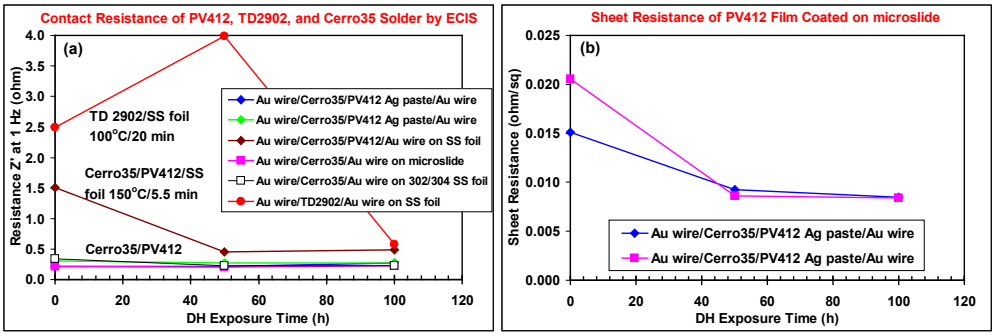

Figure 1. (a) Contact resistance from the real Z' impedance by ECIS measurements for seven samples of different contact materials made on microslide or stainless steel foil. The five curves at the bottom are DH-stable with low resistance. (b) Sheet resistance measured by four-point probe for two PV412 films coated on microslides and dotted with Cero35 solder alloy and Au wires attached.

DH Stability of Cell Components

In previous studies [2-5], we reported that bare Mo and bilayer ZnO (BZO) on glass substrates rapidly degraded in DH. In this work, we compared the DH stability of both bare and encapsulated (Dummay-1 and -2) Mo, single layer Al-doped ZnO (AZO), and BZO on glass substrates, each was cut from the same large piece substrate. Some samples of the AZO and BZO on glass had either AlNi or Ni-only grids. The test species were processed with the contact materials and Au wiring described above, and exposed to DH. In addition to the ECIS measurements, the bare samples were also measured with four-point probe for sheet resistance. The results are presented separately in the following.

3.2.1 Base Contact Mo on SLG

The Mo on soda lime glass (SLG) samples (~1.5-cm x 2.5-cm) had three contact combinations and Au wires attached to the two ends for electrical ECIS measurements. The open areas allowed for sheet resistance by four-point probe. Bare samples degraded rapidly in DH and turned bluish or gray-bluish, same as observed before. The Mo surface already became rough and/or produced fine pits as corroded by only 50 h DH, as shown in Fig. 2a, when examined under a WYKO interference optical microscope. One of the Mo/SLG samples (contacts made with PV412) became highly resistive and un-measurable by ECIS or four-point probe after 100 h DH. The other two Mo/SLG samples remained low in Z'(1 Hz) resistance (by ECIS) across the film surfaces (Fig. 2b), but four-point probe measurements showed large increases in sheet resistance from original ~$6x10^{-3}$ ohm/square to 20–90 ohms/square (Fig. 2c). In comparison, when encapsulated in the test structure with a moisture vapor permeable TPT backsheet (i.e., Dummy-1), no color change or significant resistance change (by ECIS, Fig. 2d) on the Mo/SLG sample was observed even after >1250 h DH exposure, although a number of small "dots" started to appear on the film surface after ~500 h DH. The Mo/SLG in Dummy-2 with FG-200 moisture barrier also remained constant in Z' resistance without visible surface change (Fig. 2d).

The above results raise two issues. Firstly, the large difference or irregularity in degradation rates as reflected in Fig. 2(b and c) indicates that the corrosion pathway of bare Mo by the hot steam in DH can be highly irregular – perhaps penetrating to the bulk in the PV412-Mo/SLG sample through the initially formed pits or holes (Fig. 2a) and cutting off the electrical connection so that even ECIS could not get the resistance measured, or more limiting locally and/or to the surface layers on the other two Mo/SLG samples. Secondly, the large difference in degradation rate and corrosion

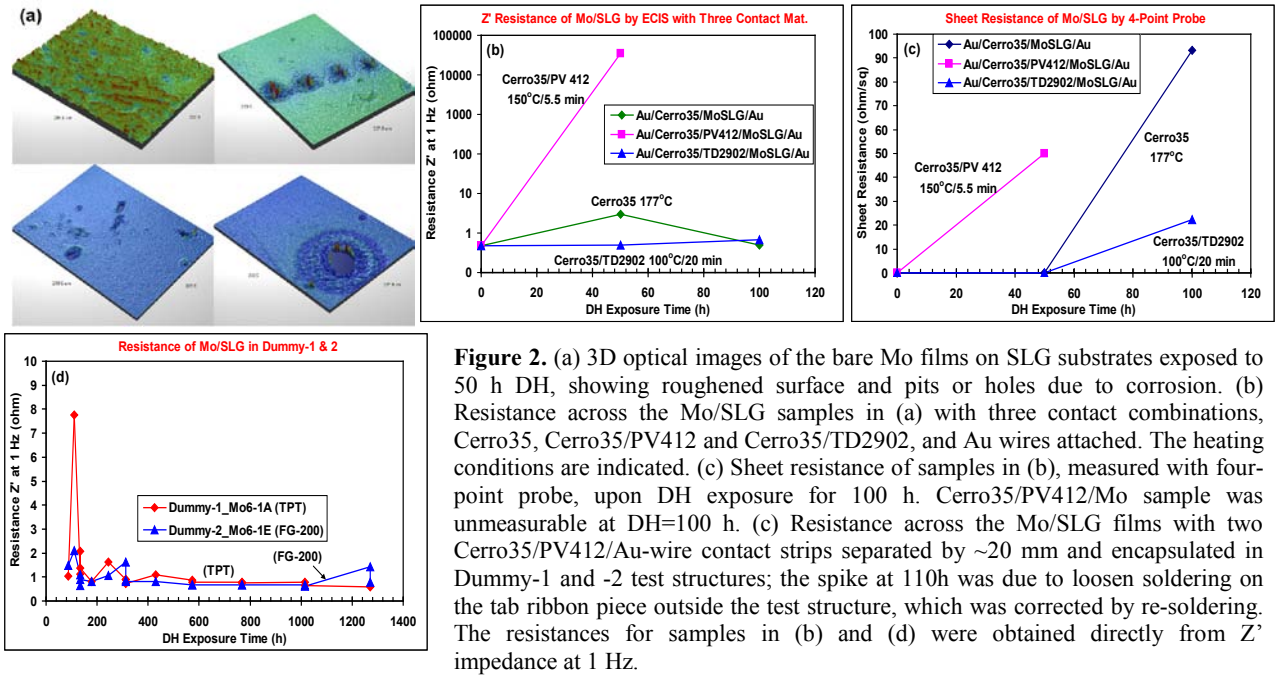

Figure 2. (a) 3D optical images of the bare Mo films on SLG substrates exposed to 50 h DH, showing roughened surface and pits or holes due to corrosion. (b) Resistance across the Mo/SLG samples in (a) with three contact combinations, Cerro35, Cerro35/PV412 and Cerro35/TD2902, and Au wires attached. The heating conditions are indicated. (c) Sheet resistance of samples in (b), measured with four-point probe, upon DH exposure for 100 h. Cerro35/PV412/Mo sample was unmeasurable at DH=100 h. (c) Resistance across the Mo/SLG films with two Cerro35/PV412/Au-wire contact strips separated by ~20 mm and encapsulated in Dummy-1 and -2 test structures; the spike at 110h was due to loosen soldering on the tab ribbon piece outside the test structure, which was corrected by re-soldering. The resistances for samples in (b) and (d) were obtained directly from Z' impedance at 1 Hz.

between bare and encapsulated samples (Fig. 2a vs. 2d) suggests the reaction mechanism is different or the reaction rate is greatly reduced in encapsulated test structure, where moisture vapor had to diffuse through the TPT layer. The observation here, together with those observed on the Set-5 with CIGS cell coupons, indicates the better testing approach is to employ an encapsulation test structure, which is more realistic as it resembles actual PV modules.

3.2.2 Front Grid Contact and ZnO Window Layer

While the "standard" trident AlNi (0.05 µm Ni + 3 µm Al) contact grid offers good conductivity to the BZO/CIGS solar cell, at issue is its DH instability due to hydrolytic corrosion and the detrimental consequence on solar cell performance when it becomes highly resistive from DH. Another possible performance-degrading factor is the loss of good conduction at the interface of AlNi and BZO. For example, it has been observed recently that, on bare CIGS cell coupons exposed to 50–100 h DH, wrinkling of the BZO layer has resulted in buckling and breaking of the AlNi grid fingerlines, causing premature cell performance failure [6]. To investigate these factors, a special grid pattern was designed with two pairs of four fingerlines interdigitated toward each other and a large square contact pad on each side for easy soldering and wiring. The "bi-grid" was used to deposit AlNi or Ni-only (0.1–0.2 µm) grid on glass, AZO/glass, BZO/glass, and CIGS cell coupons as well. The bi-grid pattern serves dual functions, allowing resistance measurement of AZO or BZO on glass or on CIGS cells as well as the cell efficiency if used on the solar cells.

Top portion of Fig. 3a illustrates the "bi-grid" contact pattern on four 0.22-µm BZO/glass pieces with 0.1 µm Ni-only (#A) and standard 3.05-µm AlNi (#B, C, D) grids. Sample pieces #A did not have Au wires attached, and pieces #B-#D were attached with Au wires using Cerro35, PV412/Cerro35, and TD2902 contact materials on the AlNi square pads. Upon quick-screen DH exposure to 100 h, sheet resistance measured by four-point probe of the Ni grid square pads showed a very small increase from ~8.5×10^{-3} ohm/square to 12.5×10^{-3} ohm/square, while the BZO films on #A–#D increased from 65–72 ohms/square to 74–85 ohms/square. However, the ECIS-measured Z' impedance/resistance for the three BZO sample pieces with AlNi bi-grids increased from original ~1.85 ohms to 40–535 ohms at DH = 50 h (Fig. 3b), and then unmeasurable (actually, messy curves) one day after DH = 100 h. In fact, during the ECIS measurements, sample piece #B became heated and cracked, and #C had a brown spot appear and spread out from the heating, as seen in the photographs. Nine days later, the two "scorched" samples became measurable with Z' (1 Hz) resistance at 56 ohms for #B and 614 ohms for #C. Sample piece #D remained highly resistive after 10 days of dry-out. These results are attributed to the "transient" behavior of the moisture-dampened BZO. DH-induced corrosion of the AlNi grids, which was clearly observed as shown in the bottom portion of Fig. 3a, could have also contributed to the magnitude of the transient phenomenon. However, similar transient behavior was observed on a large (1.5" x 3") BZO/glass sample specially designed with two Ni-only electrode bands on the top and bottom of the BZO layer at DH = 50 h and 100 h

(data/figure not shown). The moisture-soaked BZO film made it difficult to obtain good ECIS measurements on the same plane (top and bottom) and across the film, which became somewhat easier (but not completely) after allowing to dry for several days. The implication of this transient behavior is that the dampened BZO by having absorbed moisture on the surface as well as at the grain boundary can greatly hinder the electron transfer or current flow.

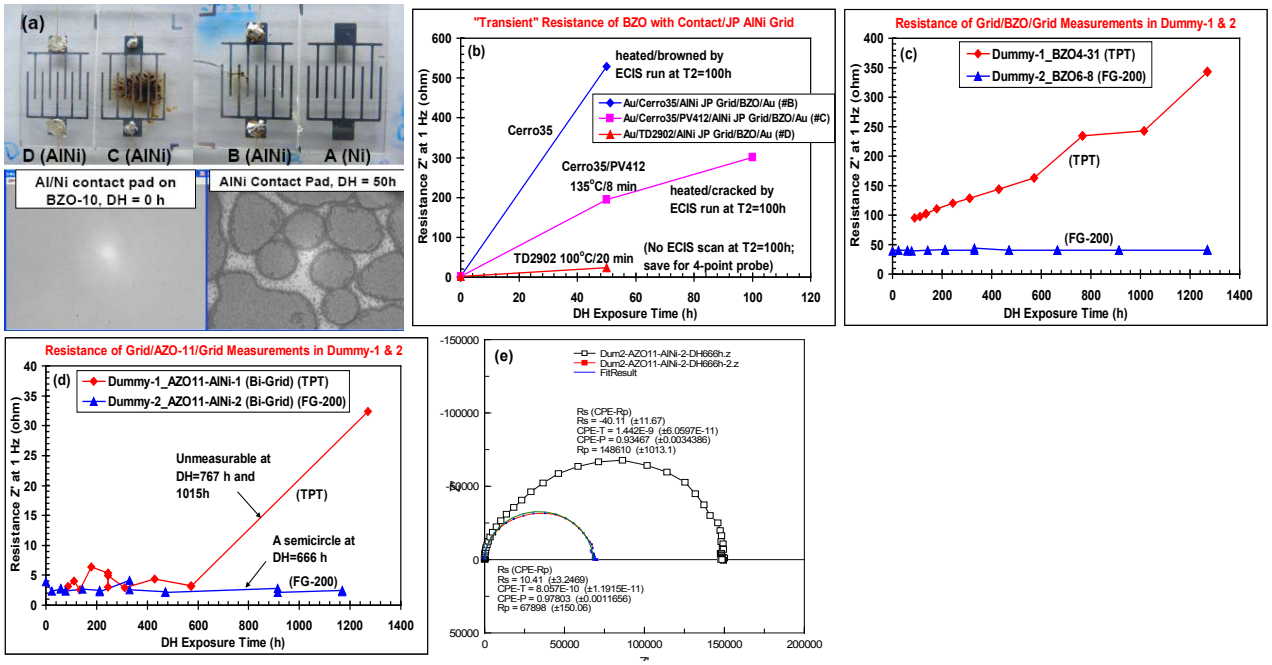

Figure 3. (a) Photographs of (top) four pieces of standard 0.22-µm BZO on glass with the "bi-grid" contact made of 0.1-µm Ni for #A and standard 3.05-µm AlNi for #B, C, and D; and (bottom) AlNi on the square pad area at DH = 0 h and 50 h. (b) "Transient" resistance for the bare samples of bi-grid AlNi/BZO in (a) at DH=50 h. The resistance was so high at DH = 100 h that samples #B and #C heated up and cracked (#B) or browned (#C) during ECIS scan. (c) Resistance of encapsulated 0.22-µm BZO/glass samples with narrow Cerro35 strips soldered on two ends separated by 18 mm, and (d) bi-grid AlNi/0.12-µm AZO in Dummy-1 and -2 as a function of DH exposure time. The sample in Dummy-1 was unmeasurable (messy curve) at DH = 767 and 1015 h. The sample in Dummy-2 also showed a transient behavior that produced a semicircle as shown in (e) for two scans at 0.0 V bias separated by 10 min.

The transient behavior, reflected as a messy curve or unmeasurable in ECIS, has not been clearly observed for the BZO/glass samples with two narrow Cerro35 contact strips and Au wires soldered on two ends, which were separated by 18 mm, and encapsulated in Dummy-1 and -2. As seen in Fig. 3c, the 0.22-µm BZO-4 in Dummy-1 with a moisture-permeable TPT backsheet shows a nearly linear increase in Z' resistance over a period of DH 1270 h, giving a degradation (resistance increase) rate of ~0.21 ohms/h. For bare BZO/glass, previous studies have showed the BZO (and AZO) could become electrically insulating within 200–500 h DH exposure as measured by Hall method or four-point probe [2-5]. With a moisture barrier FG-200 film, the degradation rate dropped to 1.05 x 10^{-3} ohm/h, as reflected from the nearly flat (blue) curve in Fig. 3c for the BZO in Dummy-2. The result clearly indicates the moisture-blocking effectiveness of the FG-200 barrier film. Single layer 0.12-µm AZO with bi-grid AlNi contacts was also studied. In Dummy-1 with TPT, the AZO-11 film showed a degradation rate of 0.14 x 10^{-3} ohms/h up to DH = 572 h, but became unmeasurable ("transient") at DH = 767 h and 1015 h and then measurable again at 1270 h. The difference in the degradation rate between the BZO and AZO in Dummies with TPT backsheet was due to the difference in contact pattern and separation (18-mm for BZO with two Cerror35 strips vs. bi-grid pattern on AZO-11). For AZO-11 in Dummy-2 with FG-200 barrier film, (blue curve in Fig. 3d), a degradation rate of 1.06 x 10^{-3} ohm/h was obtained, essentially identical to that for the BZO-6 in Dummy-1. However, a transient behavior was observed at DH = 666 h, where a semicircle was obtained for the first time as shown in Fig. 3e, indicating the presence of an R-C circuit. The semicircle size decreased on a second scan 1 h later to confirm it was not an artifact. Curve fitting gives an Rs' = 40 ohms, Rp = 148610 ohms, and C = 1.44 x 10^{-9} Farads from the semicircle of first run, which decreased to 10, 67900, and 8.06 x 10^{-10}, respectively, for the second run, indicating the metastable nature of the R-C circuit. The Rp and C are most

likely from low level moisture-dampened AZO film due to low WVTR of the FG-200 barrier film; and the Rs' = 10–40 ohms is greater than the initial 3.92 ohms prior to DH exposure, suggesting the AlNi/AZO interface may have also been affected. With higher moisture level through the TPT, the transient behavior for AlNi/AZO-11 in Dummy-1 was likely so great that it caused a messy curve (unmeasurable) at 767 h and 1015 h. However, how the transient behavior for AlNi/AZO or AlNi/BZO in the Dummies would later go away after longer DH exposure time remains unclear. On the other hand, the results shown in Fig. 3(c and d) also indicate that the contacts with Au wirings made on the Mo, AZO and BZO samples inside the encapsulated test structures for external electrical connections and ECIS measurements were DH-stable.

3.2.3 AlNi vs. Ni Contact Grid

As pointed out above, direct exposure of AlNi grid to DH resulted in hydrolytic corrosion within 50-100 h (e.g., Fig. 3a, bottom half photos), which can decrease CIGS cell performance by increased series (contact) resistance. The problem would become more serious if the ZnO bilayer wrinkled and cracked upon DH exposure, as observed on bare CIGS cell coupons [6]. Therefore, it is desirable to seek a DH-stable front contact metal to replace the AlNi so that concerns over the contact grid's DH instability issues can be reduced or eliminated. In this regard, Ni is well known to be more stable than Al against oxidation and hydrolysis. Because it has already been used at a thin layer (0.05 μm) over BZO, it is natural to test a thicker Ni-only grid for front contact. Therefore, 0.1–0.2-μm Ni-only and standard 3.0μ5-μm AlNi grids and films were deposited on different substrate for quantitative comparison. The results show substantial wrinkling, pop-up, and even delamination occurred on the AlNi films on glass and CIGS device structure (corrosion of AlNi grid was already presented above), resulting in a sheet resistance increased from 8 x 10^{-3} ohm/square at DH = 0–50 h to >1 x 10^{5} ohm/square at DH = 100 h. This is also reflected in large increase in the contact resistance (Z' at 1 Hz) measured between the AlNi film layer and the CIGS cell devices as illustrated in Figure 4a and insert. In comparison, sheet resistance of the Ni film and grid contact pad remained essentially unchanged, as shown in Fig. 4b. The average sheet resistance of BZO on these samples increased from initial ~70 ohms/square to ~95 ohms/square after 100 h DH exposure (not shwn). Accordingly, some CIGS solar cells with Ni-only grid 0.1–1.8 μm thick were prepared with mixed results. At a thin thickness of 0.2–0.3 μm, the Ni-only CIGS devices showed considerably lower efficiency due to relatively high resistance of the Ni gridlines than devices with standard AlNi grid. At 1.6–1.8 μm thick, the Ni-only CIGS devices offered comparable cell efficiency. However, due to high mechanical stress on thicker Ni layer, some of the 1.6–1.8-μm Ni-only contact grids exhibited cracking or peeled off, resulting in damaged or failed devices. More work is needed to optimize the sputtering approach and conditions for making thicker Ni contact grids with low stress and good adhesion.

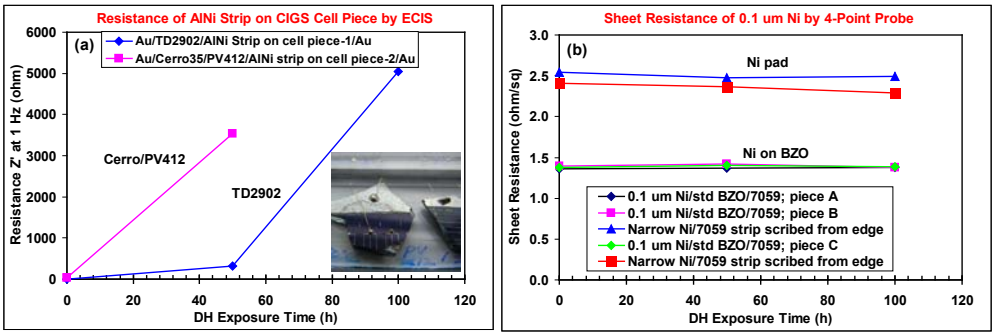

Figure 4. (a) Resistance across small CIGS cell pieces with AlNi as both contact electrodes to verify the DH-induced damages on AlNi films and contact resistance. Cerro35/PV412 and TD2902 were used on AlNi for Au wire attachment. The cell piece with Cerro35/PV412 contact was unmeasurable at D=100 h. Insert: Photograph of one of the cell piece after DH = 100 h, showing wrinkling and corrosion stain on the AlNi film. (b) Sheet resistance of 0.1-μm Ni on two glass substrates and three pieces of BZO/glass substrates upon 100 h DH exposure.

3.2 DH Stability of CIGS Solar Cells

As stated earlier, this work was designed to evaluate ECIS technology as a sensitive non-invasive analytical method to characterize the CIGS solar cells fabricated by NREL's three-stage process and monitor their DH stability in a specially designed encapsulation test structure. Characterization of DH stability of bare (unencapsulated) CIGS solar cells using conventional methods and one experiment using a test structure designed earlier were reported recently by us [6,9].

3.3.1 Cell Characteristics from ECIS Measurements

An unusual phenomenon was observed for the first time when the as-fabricated CIGS solar cells were ECIS-measured. A "jump" in the amplitude-frequency Bode plot would show in the 10–40 Hz range on some devices, causing the subsequent data points in the complex plane to scatter randomly or to shift abruptly to high Z'(real) range. A messy or skewed curve would thus result and make data extraction unreliable or curve fitting difficult. This "jump" was highly repeatable in the 10–40 Hz range; but its occurrence was not universal on all CIGS solar cells. It appeared that the jump tended to happen on devices of good quality, but not necessarily of high efficiency. It would not occur on poor-quality, low-efficiency, or degraded devices. Figure 5a demonstrates the skewed and normal curves in the Z"-Z' complex plane for five devices on four different cell coupons, with the corresponding Bode plots and cell efficiency given in Fig. 5b. The "jump" seems to relate to yet-unidentified potential barrier in the devices. This potential barrier was overcome to obtain a good semicircle in the complex plane for most cells when a forward bias at 0.25 V was applied; some devices required a 0.30 V bias. However, the "jump" was also observed on pure capacitors, for example, a "jump" at 316 Hz appeared when a 5–20 pF or a 150–200 pF capacitor was measured in the same way, which caused similar messy curve in the complex plane plot. Therefore, the "jump" by a CIGS device may be a clear indicator of nearly pure-capacitor quality. Furthermore, ECIS analysis was found to be able to easily distinguish cells of different R-C quality/property but similar cell efficiency. For example, Fig. 5c compares the semicircles for five devices on the same cell coupon C2529-13, with two cells not biased and three biased at 0.30 V. The five devices had cell efficiency within a 13–15% range, but exhibited large variation in the ECIS responses. This kind of variation was observed for many of the CIGS cell coupons studied.

The semicircles were obtained in the ECIS scan because the CIGS solar cells, like many other kind of solar cells (e.g., c-Si), are constituted with a p-n junction and a depletion width forming a capacitor and a parallel resistance, which, along with the contact series resistance, can be represented by a simple equivalent circuit as shown in Scheme 1 above, i.e., Rs'-(Rp-C). The three parameters can be extracted from the semicircle and by using an appropriate curve fitting. Therefore, the large variations seen on the semicircles and the Bode plots in Fig. 5 clearly reflect the variations in the contact/bulk resistance and p-n junction details, or Rs'-(Rp-C), of the devices. These observations indicate two points that are mutually contradictory. On one hand, it shows that ECIS analysis is highly sensitive to the (Rp-C) difference among devices; on the other hand, the obvious variation for devices even on the same cell coupon indicates the non-uniformity of devices, a likely consequence of compositional and/or device quality non-uniformity. The latter unwillingly imposes a restriction on the ECIS analysis for the CIGS solar cells; that is, individual analysis has to be performed for individual devices to monitor and track the performance and DH stability trend. A simple generalization of the analysis results may not be entirely accurate or reliable.

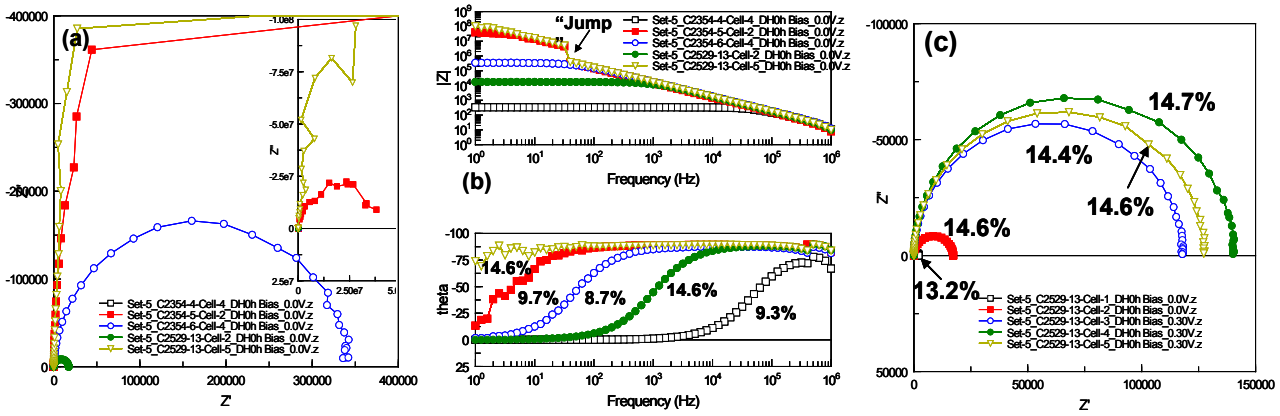

Figure 5. (a) Complex plane plots for five CIGS solar cells from four cell coupons, C2354-4, -5, -6 and C2529-13, at DH = 0 h, showing two skewed curves (insert) due to the "jump" at 39.8 Hz, one large, and three small semicircles. (b) Corresponding impedance amplitude (top) and phase angle (bottom) vs. frequency Bode plots, whereas the "jump" on two curves and efficiencies of the five cells are labeled. (c) Semicircles for five cells on the same coupon of C2529-13 at DH = 0 h, showing the large variation of impedance response due to variation of cell quality while cell efficiencies are within a narrow range of 13.2%–14.7%.

3.3.2 DH-Induced Degradation and Curve Fitting with Equivalent Circuit Models

Although Rs' values can be obtained from the Z'(real) at 1M Hz for convenience, the quality of the actual Z"-Z' curve for a degrading solar cell may be quite noisy or non-linear in the low-frequency region, making determination of Rp from Z'(real) at 1 Hz (i.e., sum of Rs' and Rp) unreliable. Besides, the purpose of this study is intended to seek the insight of what happens to the CIGS devices when they are degraded by DH exposure. Therefore, curve fitting is preferred so that more accurate or reliable values of Rs', Rp and C can be obtained and compared to the values of Z'(real) at 1 Hz and 1M Hz. Due to the very large volume of data files (several hundreds), the two built-in "instant fit" functions, Rs'-(Rp-C) and Rs'-(Rp-CPE) equivalent circuits, were used directly for curve-fitting manually and individually with generally satisfactory results. The CPE stands for "constant phase element," a factor indicating the non-ideal quality of a capacitor (or an R-C circuit) that can be affected by surface roughness, porous structures, varying thickness or composition, non-uniform current distribution, and/or inhomogeneous reaction rates on an electrode surface [13,21,22]. Quality of the curve fit was determined from the degree of curve superimposition as well as the error percentages of the parameters. The Rs'-(Rp-CPE) fit would produce two parameters: CPE-T, which is essentially the capacitance (C), and CPE-P, which typically is < 1.0 (1.0 for an ideal Rs'-(Rp-C) circuit or a pure capacitor, and 0 for a pure resistor) and can be viewed as a measure of "depression" degree on the "p-n junction capacitor" due to certain physical effects. For the initial and slightly degraded cells, curve fitting with either model was found satisfactory and gave similar results with CPE equal to or very close to 1.0 (not shown) because the semicircles (or the p-n junction capacitors) were not or little perturbed. As the cells degraded further and the semicircles became more "depressed," curve fit using Rs'-(Rp-CPE) was required to obtain a good fit. Figure 6a illustrates the steady decrease in the size of Z"-Z' semicircles for cell#5 on C229-13 coupon, which is common for most of the degrading cells, due to DH-induced degradation. However, a few cells showed semicircle size increased first then largely decreased in later stage, as demonstrated in Fig. 6b for cell#7 on C2354-4 coupon. Figure 6c gives an example of curve fitting, comparing the fit quality using the two models Rs'-(Rp-C) and Rs'-(Rp-CPE) for a much-depressed semicircle for cell#7 on C2354-4 coupon at DH=774 h (Fig. 6b). For medium to highly degraded cells, the depressed semicircles are better fit with the CPE model than the Rs'-(Rp-C) (Randles cell) model, which is best for unexposed and lightly degraded cells.

3.3.3 Correlation of I-V and ECIS Results

Correlation between photovoltaic performance and impedance spectroscopy was reported for dye-sensitized solar cells by Fabregat-Santiago et al. [23]. To correlate the DH-induced degradation on CIGS solar cell I-V performance and changes in ECIS parameters, cell#5 on the C2529-13 cell coupon (with 0.5-μm AZO) in the encapsulated Set-5 test structure was selected as an illustrative example given in Fig. 7. The six cells on the C2529-13 exhibited efficiency

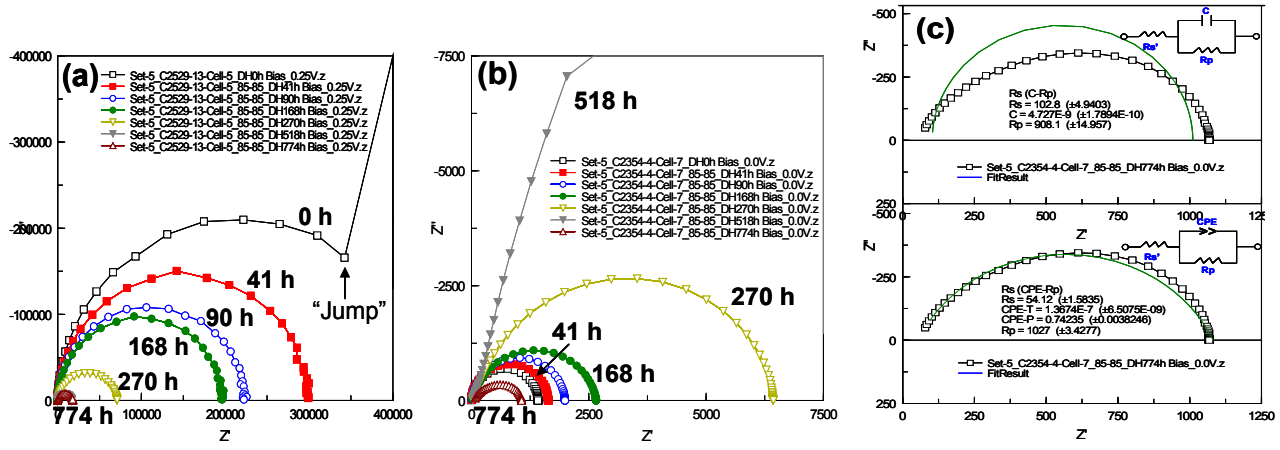

Figure 6. (a) Complex plane plots obtained with a 0.25 V forward bias for cell#5 on C2529-13 coupon in the encapsulated Set-5 at DH = 0, 41, 90, 168, 270, 518, and 774 h, showing the continued decrease in the semicircle size. (b) Semicircles for cell#7 on C2354-4 coupon in Set-5 at the same DH exposure intervals. The semicircle size increased to DH = 518 h and then largely decreased at DH=774 h. In both cases, the cell efficiency steadily decreased as the DH exposure time increased. (c) Example of curve fitting quality of a "depressed" semicircle for cell#7 on C2354-4 coupon at DH = 774 h separately using the Rs'-(Rp-C) (top) and Rs'-(Rp-CPE) (bottom) equivalent circuit model with a constant phase element (CPE). The solid curves are fit results.

decrease from original 13%–16% (measured under the topcover glass) to 0%–6% in an irregular pattern after being exposed to the DH moisture vapor (permeated through the TPT backsheet) for 774 h. Cells#2, 4 and 5 showed vey similar trend. Winkling and cracking of the BZO layer was extensive over the entire area of cells#1, 2 and 3, and partial on cell#4. BZO layer wrinkling was seen over the entire cell area of cells #1-4, but not on cells #5 and 6. For bare cell coupons, a 50–100 h DH exposure could induce extensive wrinkling, cracking, and delamination on the BZO layer and the AlNi grids over it [6]. Curve fitting using the Rs'-(CPE–Rp) equivalent circuit model was performed to extract the parameters of Rs', Rp, CPE-T (i.e., C), CPE-P (see Fig. 6c), and maximum frequency from the Z"-Z' semicircles and calculate the effective minority lifetime (time constant) by Rp*C [13,15-17,21,22]. However, the Rp*C is the "overall" magnitude, without trying to separate the recombination and diffusion terms.

Figure 7b shows the plot of I-V parameters (Voc, Jsc, FF, efficiency) normalized to that at DH=0 h, and Fig. 7c shows the plot of normalized Rs and Rsh from derived from light I-V measurements up to 518 h. The initial Rs and Rsh values were 1.96 and 2278 ohm-cm^2 respectively, and became unreliably very large at DH=774 h as derived from three or four data points on the LIV curves. As seen in Fig. 7(b and c), cell FF and efficiency dropped largely after DH = 270 h, in parallel to the large increase in Rs and Rsh. Jsc was fairly steady till DH = 518 h, but dropped suddenly to 0.03 mA/cm^2 at DH = 774 h, indicating a breakdown in the current flow pathway (i.e., electrical conduction) that also gave very high Rs. The Voc was more consistent over the course of 774 h DH exposure. On the ECIS side, Fig. 7d shows the plots of Rp (minority carrier recombination/diffusion resistance), CPE-T (the capacitance, same as C), CPE-P (the "depression" factor), and the Rp*C (i.e., CPE-T) lifetime in a logarithmic scale. Figure 7e shows the plots for the pairs of Rp and Z'(1 Hz) and of Rs' and Z'(1M Hz). Note that the initial data points at DH = 0 h for Rp, C, and Rp*C from curve fitting and Z'(1 Hz) from measurement are not used because of the "jump" (Fig. 6a). Rp from curve fitting matched quite well with Z'(1 Hz) and in a way was related to the Rsh, and the Rs' deviated somewhat from Z'(1M Hz) by 0–6 ohms but was more dependable. The measurements were carried out at a 0.25 V forward bias. The ECIS results confirmed further the contact/bulk series resistance (Rs') increased quickly, while Rp decreased steadily from original 4.18 x 10^5 ohms to 1.77 x 10^4 ohms. The capacitance (CPE-T or simply C) decreased from an original 1.12 x 10^{-8} F to 7.03 x 10^{-9} F at DH = 168 h and then increased to 2.20 x 10^{-8} F at DH =774 h, indicating the capacitance of the "p-n junction capacitor" gradually

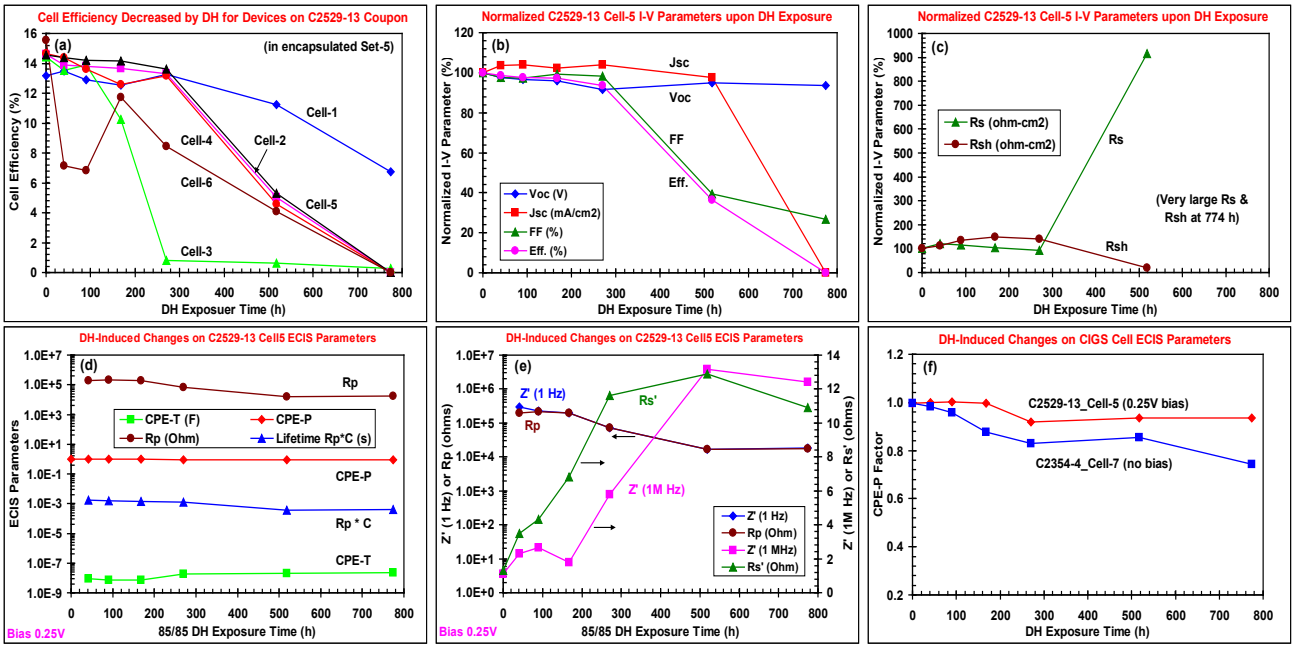

Figure 7. Correlation of I-V results with ECIS results for cell#5 of C2529-13 cell coupon exposed to DH for 774 h. (a) Efficiency degraded for all the six cells on the coupon, (b) normalized I-V parameters (Voc, Jsc, FF, and efficiency) for cell#5, (c) normalized series resistance (Rs) and shunt resistance (Rsh), (d) curve-fitting extracted ECIS parameters, Rp, CPE-T, CPE-P, and calculated lifetime (time constant), Rp*C (i.e., CPE-T), for cell#5, (e) curve-fitting extracted Rs' and Rp plotted with the Z' resistance obtained at 1 Hz and 1M Hz in the measurements, and (f) plots of DH-degraded CPE-P factor for two cells, #5 on C2529-13 and #7 on C2354-4 coupon. The ECIS measurements for C2529-13 cell#5 were performed with a 0.25 V bias to obtain the semicircles shown in Fig. 6a. Curve fitting used the Rs'-(CPE–Rp) equivalent circuit model.

increased. The Rp*C lifetime (time constant) was decreased accordingly due to large change in Rp. Meanwhile, the CPE-P "depression" factor decreased steadily from 1.0 to 0.93 at DH = 774 h, as shown in Fig. 7(d and f). Greater "depression" of the CIGS solar cells' "p-n junction capacitor" was obtained for other DH-degraded devices in Set-5, which decreased to 0.74 at DH = 774 h for the cell#7 on C2354-4 cell coupon with 0.12-μm AZO as illustrated by the blue curve in Fig. 7f. All the cells on C2354-4 coupon degraded faster than C2529-13. Although most of the degraded cells display trend of change in ECIS parameters similar to that of C2529-13 cell#5 above, there were a few cells that showed largely increased Rp, little decreased C, and hence increased Rp*C [6]. Overall the changes in Rs', Rp, CPE-T, and Rp*C indicate that the BZO/AlNi electrical contact has degraded and the cell's "p-n junction capacitor" (depletion layer) has undergone certain physical changes. The decreasing trend in CPE-P suggests the junction capacitor had been affected probably by increased surface roughness, porous or varying thickness or composition, and non-uniform current distribution induced by DH hydrolysis at the CIGS/CdS layers and interface. The exact physical mechanisms are not clear, however.

Using the data for Fig. 7 above, we also attempt to seek correlation, and offer adequate physical interpretations, of the ECIS results with I-V results for the CIGS solar cells degraded by DH exposure by normalization of the data, which are then plotted to find the parallel trends or relationship among various parameters. The quality of correlation treated in this manner will be obviously affected by the quality of the original data, especially the *initial* data at DH=0 h, however. This is simply because the value of initial data will determine the magnitude of the ratio. In this regard, the initial data points for Rp and Rp*C from curve fitting and Z'(1 Hz) from measurement are not used because of the "jump" (e.g., Fig. 6a); instead, the data at DH=41 h were used as the initial data for calculating the ratios. The processed results are grouped into three plots for easier viewing. In Fig. 8a, the two curves for Voc and CPE-P appear to match well, and the Rp*C curve aligns reasonably well with FF and efficiency (Eff.) curves and less with Jsc curve; but the five curves (including Rp) are generally in a similar trend of changes. These seem to be reasonable because CPE-P is a measure of "depression" of the junction capacitor (depletion width), a small decrease in the junction capacitor should result in also a small change in Voc. Because Rp is the minority carrier recombination/diffusion resistance and the Rp*C is the lifetime, they should impact directly on the current density and efficiency. Figure 8b shows that the curve-fit Rp is, and should be, in good parallel relationship with the measured Z'(1 Hz) because they are supposed to be the same. Their alignment with Rsh is not so satisfactory due to the fairly high uncertainty of Rsh values that were derived from only a few data points from the light I-V curves by the measurement program. The Rsh values were observed to change significantly when a device was measured repeatedly for three to four times. The Rp and Rsh should also be in parallel because they account for or reflect the minority carrier recombination/diffusion resistance. In Fig. 8c, the series resistances Z'(1M Hz) and Rs' (from ECIS) are in parallel as expected, and Z'(1M Hz) is also in good agreement with Rs (from I-V). Although the CPE-T (or C) curve, capacitance for the p-n junction capacitor, seems to be in good agreement with the Rs' curve in Fig. 8c, it is probably better represented as in Rp*C that correlates well with FF and Eff. curves (Fig. 8a). Accordingly, as a first-time effort, the ECIS results are found to correlate reasonably well with the I-V results, although more in-depth material analysis and insightful physical interpretations are still needed. This is particularly true on the CPE-P factor – what and how chemical and physical changes can induce "depression" of the junction capacitor.

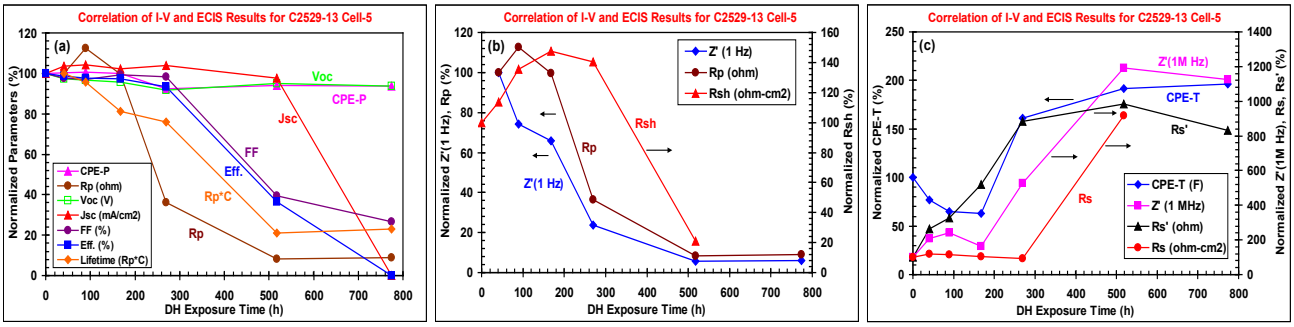

Figure 8. Normalized plots in three groups in an attempt to correlate I-V results with ECIS results for C2529-13 cell#5 given in Fig. 7. (a) Grouped plot for I-V's Voc, Jsc, FF, efficiency with ECIS's Rp, Rp*C, and CPE-P. (b) Grouped plot for I-V's Rsh with ECIS's Rp and Z'(1 Hz). (c) Grouped plot for I-V's Rs with ECIS's CPE-T, Rs', and Z'(1M Hz).

3.3.4 ECIS Differentiation of "Conduction-Failed" Cells from "Junction-Failed" Cells

An important issue related to the performance degradation of (CIGS) solar cells induced by accelerated environmental stresses (e.g., DH conditions) needs to be clarified. It will be useful to know whether the CIGS solar cells are truly dead, damaged, or shorted at the p-n junction level in addition to electrical conduction degradation/failure by DH exposure, or whether the solar cells' I-V performance degradation is mainly due to electrical conduction degradation/failure at the ZnO/AlNi and Mo electrodes. Conventional I-V measurements may not be able to attain the differentiation. In contrast, ECIS analysis offers the possibility. Figure 9a shows the Z"-Z' complex plane plots for some of the cells on the cell coupons in the encapsulated Set-5, indicating these cells were shorted, damaged, or highly degraded at different DH exposure time. These cells produced very low to zero efficiency. The degradation on these cells' electrical contact parts varies, as inferred from the Z'(real) resistances (~2–27 ohms). Cell damages or shorting by DH on these cells are apparently more important than electrical contact degradation. However, ECIS analysis results indicate that, at DH=774 h, some devices still maintained good R-C semicircles with high to very high Rp and C, typical of good-quality cells, despite they lost a large percentage to 100% of efficiency. Figure 9b illustrates the Z"-Z' complex plane plots obtained at 0.25 V bias for four of such cells, two on C2354-5 with 0.36-µm AZO and two on C2529-13 cell coupon with 0.50-µm AZO. The insert in Fig. 9b shows the portion of Z'(1M Hz) resistance of these four cells, ranging from ~9 ohms to ~50 ohms, indicating the presence of electrical conduction degradation. These cells were difficult to get good I-V measurements, hindered either by an odd I-V curve and/or by a very slow voltage scan, which produced very large Rs and Rsh, a clear indication of electrical conduction problem. Unless there was an electrical open circuit, ECIS measurements using a 10 mV AC amplitude were not hindered by this problem, however. These cells with low to zero efficiency but good R-C semicircles most likely continued to possess good p-n junction even as their electrical conductions were largely degraded. The degradation in electrical conduction is likely on BZO and AlNi (Fig. 3) and not on Mo because Mo/SLG in encapsulated Dummy-1 with TPT backsheet did not show significant change after >1270 h DH exposure (Fig. 2c). One way to confirm the assessment that the CIGS/CdS junction on these cells is still alive is, as we planned, to remove the four cell coupons from the Set-5 test structure and re-fabricate the cells with new CdS, BZO, and AlNi grids [9]. Finally, it is worth noting that an I-V dead cell (C2529-13 cell #6 at DH=774h) gave a double semicircle, which was observed for the first time, as shown in Fig. 9c and marked with curve fit parameters using both circuit models for the two scans at 0.0 V and 0.30 V bias respectively. The unusual behavior appears to provide further evidence of previously discussed points: the first (left) semicircle is attributed to the DH-degraded cell (as in Fig. 8a) and the second (right) semicircle is attributed to the capacitance-forming consequence on the BZO/AlNi layers (as in Fig. 3e).

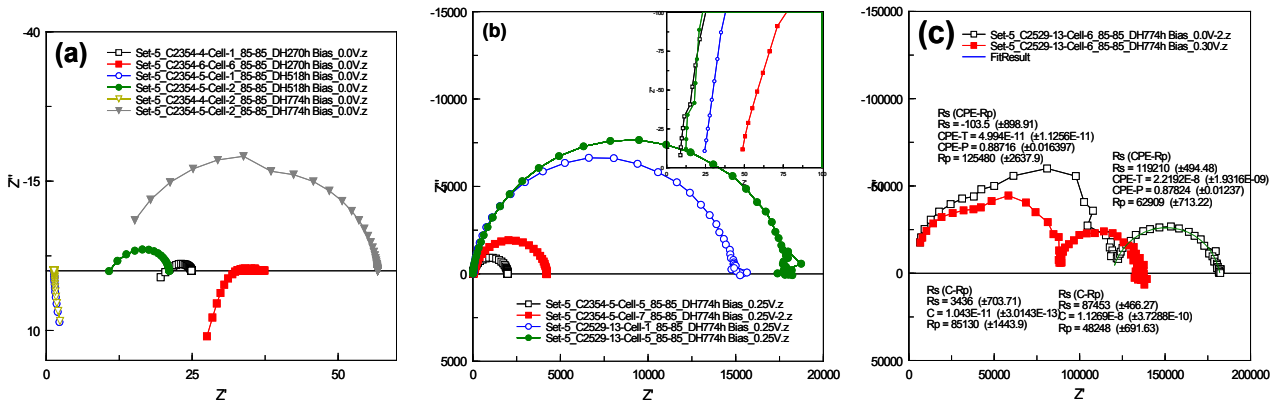

Figure 9. (a) Complex plane plots for six cells on three CIGS coupons exposed to DH at 270, 518 and 774 h, respectively, showing shorted (vertical lines), mostly shorted (red curve), depressed, and highly depressed cells. Efficiencies of these cells are in the order (from top down on the datafile list) of 1.73, 0.95, 0.0, 1.47, 0.0, and 2.39% (this showed an unreliable odd I-V curve). (b) Good semicircles obtained with 0.25 V bias for four cells on two cell coupons at DH=774 h. The insert is a blow-up to show the increased Rs', Z'(1M Hz). The cell efficiencies are in the order (from top down) of 0.0, 1.55, 6.72, and 0.0%. (c) Two double semicircles obtained for cell#6 on C2529-13 coupon at DH=774 h. The cell was dead at 0.0% efficiency, and the two scans with 0.0 V and 0.30 V bias were separated by 1 h. Curve fitting results for both pairs of double semicircle are included.

4. CONCLUSIONS

We have conducted a fairly comprehensive study employing (electrochemical) impedance spectroscopy (ECIS) to characterize a large sample matrix, including various contact materials, processing conditions, CIGS cell components and devices, which used those contact materials for external electrical connection, for their DH stability in both bare and encapsulated test structures. The important results are outlined in the following:

- DH-stable contacts are obtained with a Ag paste, processed briefly at 150^{o}C, and a low-melting-point solder alloy, realizing reliable external electrical connection with soldered Au wires on the encapsulated test structures.
- Mo on SLG shows significant difference in DH-induced reaction between bare and encapsulated states. Essentially little to no degradation was observed in encapsulated test structure with a moisture-permeable TPT backsheet that was exposed for over 1270 h.
- Bi-layer ZnO (BZO) in the same encapsulated test structure showed a degradation rate (resistance increase) of ~0.21 ohm/h with a moisture-permeable TPT backsheet, which dropped to ~1.0 x 10^{-3} ohm/h when a moisture barrier film FG-200 was used. The BZO on CIGS solar cells tends to wrinkle and crack sooner or later upon DH exposure, whether in bare or encapsulated states.
- The standard 3.05-μm AlNi contact grids are readily degraded or corroded by DH, much faster on bare samples.
- Ni-only contact grids are DH-stable even on bare samples. At 1.6–1.8 um thick, Ni-only CIGS solar cells perform comparably to the standard 3.05-μm AlNi grids. However, cracking and/or peel-off of thicker Ni gridlines due to high mechanical stress remains an issue to be solved.
- The AlNi/BZO layers are the primary degrading factors on electrical conduction responsible for DH-induced CIGS performance loss. "Transient" behavior of very high resistance on dampened AZO and BZO is likely due to hydrolytic "capacitor-forming" reactions by DH on both the BZO layer and AlNi/(or Ni/)BZO interface.
- ECIS is able to extract series resistance (Rs'), minority carrier recombination/diffusion resistance (Rp), and diffusion/depletion capacitance (C) via curve fitting with equivalent circuit models. These parameters show the large variation of individual CIGS cell characteristics and their changes provide insight of solar cell degradation.
- ECIS analysis show that the CIGS solar cells exposed to DH can result in shorting, damage, or depression of the cells' p-n junction, in addition to the AlNi/BZO degradation. However, some cells with 0.36 or 0.50-μm AZO are likely to have performance degraded partly by electrical conduction loss on AlNi/BZO. ECIS is capable of differentiating such "conduction-failed" from "junction-failed" cell degradation.
- ECIS results appear to correlate reasonably well with the I-V results on performance degradation as a function of DH exposure time.

Accordingly, we have demonstrated the power of ECIS as a sensitive, non-invasive and non-destructive analytical technology as well as its highly complementary capability to conventional I-V measurements in the characterization of CIGS solar cell characteristics and performance reliability.

ACKNOWLEDGMENTS

The authors thank D. Gallapsie for lending the ECIS system. S. Glynn, C. DeHart and R. Sandaramoorthy are thanked for some sample preparations or processing. This work was performed at the National Center for Photovoltaics under DOE Contract No. DE-AC36-08GO28308 with the National Renewable Energy Laboratory.

REFERENCES

[1] K. Whitfield, "Common Failure Modes for Thin-Film Modules and Considerations toward Hardening CIGS Cells to Moisture – A "Suggested" Topic," Proc. 2010 PV Module Reliability Workshop, Feb. 16-17, 2010, Golden, CO.

[2] J. Pern and R. Noufi, "An Investigation of Stability Issues of ZnO and Mo on Glass Substrates for CIGS Solar Cells upon Accelerated Weathering and Damp Heat Exposures," DOE SETP Review Meeting, Denver, CO., April 17-19, 2007. http://www1.eere.energy.gov/solar/review_meeting/pdfs/p_9_pern_nrel.pdf.

[3] R. Sundaramoorthy, F.J. Pern, C. DeHart, T. Gennett, F.Y. Meng, M. Contreras, and T. Gessert, "Stability of TCO Window Layers for Thin-Film CIGS Solar Cells upon Damp Heat Exposures – Part II," (b) F.J. Pern, S.H. Glick, X. Li, C. DeHart, T. Gennett, M. Contreras, and T. Gessert, "Stability of TCO Window Layers for Thin-Film

CIGS Solar Cells upon Damp Heat Exposures – Part III," *Proc. SPIE PV Reliability Conference*, 8/2-6/2009, San Diego, CA.

[4] F.J. Pern, S.H. Glick, R. Sundaramoorthy, B. To, X. Li, C. DeHart, S. Glynn, T. Gennett, R. Noufi, and T. Gessert, "Damp-Heat Instability and Mitigation of ZnO-Based Thin Films for $CuInGaSe_2$ Solar Cells," *Proc. 35 IEEE PVSC*, 6/20-25/2010, Honolulu, Hawaii.

[5] F.J. Pern, B. To, S.H. Glick, R. Sundaramoorthy, C. DeHart, S. Glynn, C. Perkins, L. Mansfield, and T. Gessert, "Variations in Damp Heat-Induced Degradation Behavior of Sputtered ZnO Window Layer for CIGS Solar Cells," Proc. SPIE PV Conference #7773 "Reliability of Photovoltaic Cells, Modules, Components, and Systems III", 8/1-5/2010 San Diego, CA.

[6] F.J. Pern, L. Mansfield, C. DeHart, S.H. Glick, F. Yan, and R. Noufi, "Thickness Effect of Al-Doped ZnO Window Layer on Damp-Heat Stability of $CuInGaSe_2$ Solar Cells," 37th IEEE PVSC, 6/21-6/25/2011, Seattle, WA.

[7] F.J. Pern, B. Egaas, B. To, C.-S. Jiang, J.V. Li, S. Glynn, and C. DeHart, "A Study on the Humidity Susceptibility of Thin-Film CIGS Absorber," *Proc. 34 IEEE PVSC*, 6/7-12/2009, Philadelphia, PA.

[8] R. Sundaramoorthy, F.J. Pern and T. Gessert. "Preliminary damp-heat stability studies of encapsulated CIGS solar cells," *Proc. SPIE PV Conference # 7773 "Reliability of Photovoltaic Cells, Modules, Components, and Systems III,"* 8/1-5/2010, San Diego, CA.

[9] R. Sundaramoorthy, F.J. Pern, G. Teeter, Jian V. Li, M. Young, D. Kuciauskas, B. To, F. Yan, S. Johnston, R. Noufi and T.A. Gessert, "Influence of Damp Heat on The Electrical, Optical, and Morphological Properties of Encapsulated $CuInGaSe_2$ Devices," Proc. 37 IEEE PVSC, June 21-25, 2011, Seattle, WA.

[10] J. Wennerberg, J. Kessler, M. Bodegard and L. Stolt, "Damp Heat Testing of High Performance CIGS Thin Film Solar Cells," Proc. 2nd World Conference and Exhibition on Photovoltaic Energy Conversion, July 6-10, 1998, Vienna, Austria, pp. 1161-1164.

[11] J. Klaer, R. Klenk, A. Boden, A. Neisser, C. Kaufmann, R. Scheer, H.-W. Schock, "Damp Heat Stability of Chalcopyrite Mini-Modules," Proc. 31st IEEE PVSC, 2005, pp. 336-339.

[12] F.J. Pern, F. Yan, L. Mansfield, S. Glynn, M. Rekow, and R. Murison, "Performance Characterization and Remedy of Experimental $CuInGaSe_2$ Mini-Modules," 37th IEEE PVSC, 6/21-6/25/2011, Seattle, WA.

[13] "*Impedance Spectroscopy – Emphasizing Solid Sate Materials and Systems*," J. Ross MacDonald ed., John Wiley & Sons, New York, 1987. Also see "Constant Phase Element" in Chapters 1 and 2.

[14] M.S. Suresh, "Measurement of Solar Cell Parameters using Impedance Spectroscopy," *Solar Energy Materials and Solar Cells,* **43,** 1996, pp. 21-28.

[15] Mora-Sero, G. Garcia-Belmonte, P.P. Boix, M.A. Vazquez, and J. Bisquert, "Impedance spectroscopy Characterisation of Highly Efficient Silicon Solar Cells under Different Light Illumination Intensities," *Energy Environ. Sci.*, **2**, 2009, pp. 678–686.

[16] J. Bisquert, "Theory of the Impedance of Electron Diffusion and Recombination in a Thin Layer," J. *Phys. Chem. B,* **106**, 2002, pp. 325-333.

[17] J. Bisquert, "Impedance Spectroscopy Applied on Solar Cells," a presentation at the Nordic Workshop on Solar Electricity, Sonnerupgaard Gods, Denmark, 27-29 April 2004.

[18] H. Bayhan and A. S. Kavasoglu, "Admittance and Impedance Spectroscopy on $Cu(In,Ga)Se_2$ Solar Cells, *Turk J. Phys.* **27**, 2003, pp. 529-535.

[19] H. Bayhan and A. S. Kavasoglu, "Study of $CdS/Cu(In,Ga)Se_2$ Heterojunction interface Using Admittance and Impedance Spectroscopy," *Solar Energy*, **80**, 2006, pp. 1160-1164.

[20] Meier, S.H. Glick, and F.J. Pern, "Impedance Spectroscopy as a Non-Invasive Analytical Method for Monitoring Solar Cell Degradation," NCPV Photovoltaics Program Review, *Proc. of 15th Conference*, M. Al-Jassim, J.P. Thornton, and J. M. Gee ed., CP462, Denver, CO, Sept., 1999, pp. 661-666. American Institute of Physics, Woodbury, New York.

[21] (a) "Explaining a Constant Phase Element (CPE)," http://www.consultrsr.com/resources/eis/cpe2.htm, and the references therein. (b) "Constant phase element," http://en.wikipedia.org/wiki/Constant_phase_element.

[22] Help menu on equivalent circuits, instant curve fitting function and constant phase element in the ZView program (ver. 3.2c) from Scribner Associates, Inc.

[23] F. Fabregat-Santiago, J. Bisquert, E. Palomares, L. Otero, D. Kuang, S. M. Zakeeruddin, and M. Graetzel, "Correlation between Photovoltaic Performance and Impedance Spectroscopy of Dye-Sensitized Solar Cells Based on Ionic Liquids," *J. Phys. Chem. C,* **111**, 2007, pp. 6550-6560.